Progress In Electromagnetics Research, PIER 72, 21–37, 2007

PERFORMANCE EVALUATION OF SEPARATED APERTURE SENSOR GPR SYSTEM FOR LAND MINE DETECTION

K. Moustafa and K. F. A. Hussein

Microwave Engineering Department
Electronics Research Institute (ERI)
Dokki, Cairo, Egypt

Abstract—In this paper, the performance of the separated-aperture sensor working as ground-penetrating radar (GPR) is assessed over the operating frequency band. The capability of the separated-aperture sensor to detect buried targets is examined by evaluating and comparing the electromagnetic coupling between the transmitting and receiving antennas in two cases: (i) when the system is placed over an empty ground and (ii) when it is placed over a ground inside which a practical target is buried at the proper depth. The finite-difference time-domain (FDTD) method is used for electromagnetic simulation. The results concerning the coupling between the transmitting and receiving antennas are presented considering various practical parameters such as the operating frequency, the electric properties of the ground soil and the buried target, and the depth at which the target is buried under the ground surface. It is shown that target detectability using the separated-aperture sensor is strongly dependent on all of the above parameters.

1. INTRODUCTION

Optimum performance of GPR systems is obtained only by taking into account details of the target geometry and the nature of the ground. Many forms of GPR antennas are used for buried land mine detection, for example, bow-tie [1, 2, 13, 15], resistively loaded Vee dipole [3, 4] and ultra wide-band (UWB), dual-polarized, dielectric-loaded horn-fed bow-tie (HFB) antennas [5]. The separated-aperture sensor has been introduced in [6] as a GPR system for detection of land mines. One of the major advantages of this system is its dependence on a continuous-wave operation of single frequency for mine detection. This avoids the difficulties encountered in the process of detecting ground-buried

mines, which result from the necessity of accounting for the dispersive properties of the ground soils. Thus, unlike the other types of GPR systems that depend on short pulse detection, the separated-aperture sensor does not require a wideband antenna for the process of mine detection. Narrow-band transmitting and receiving dipole antennas are used in the separated-aperture sensor; each of which is partially covered by a corner reflector. A metallic septum with the appropriate length keeps the two antennas separated from each other.

The mechanism of target detection in the separated-aperture sensor GPR depends on a continuous-wave operation, where the amount of electromagnetic coupling between the isolated transmitting and receiving antennas is used to indicate the presence or absence of a buried target. Thus a single-frequency microwave-source attached to the transmitting dipole antenna and a power meter, with the appropriate sensitivity, attached to the receiving antenna are enough for good operation.

Some examples showing the capability of this system to detect land mines are presented in [6]. However, the investigations presented in [6] are not complete and other practical situations are needed to provide complete assessment of the system performance.

This paper provides elaborate discussions, based on accurate results, to investigate the performance of the separated-aperture sensor in detecting buried targets in practical situations showing various types of targets and ground soils.

2. SEPARATED-APERTURE SENSOR CONSTRUCTION AND OPERATION

The separated-aperture sensor has been used in GPR systems [6]; it consists of two parallel dipole antennas (one for transmission and the other for reception) housed in reflectors that are separated by a metallic septum as shown in Fig. 1. When the sensor is over empty ground, the coupling between the transmitting and receiving antennas $|S_{21}|$ is very small because of the conducting septum and reflectors that partially cover the two antennas and, hence, prevent the direct coupling between them. As the sensor is moved over a buried target, the target reflects a portion of the signal radiated by the transmitting antenna back to the receiving antenna, thus increasing the coupling between the antennas. The increase in the coupling is used to detect the presence of the buried target.

Fig. 1 shows the dimensions of the separated-aperture sensor (corner reflectors, septum, and dipole antennas) considered in this paper.

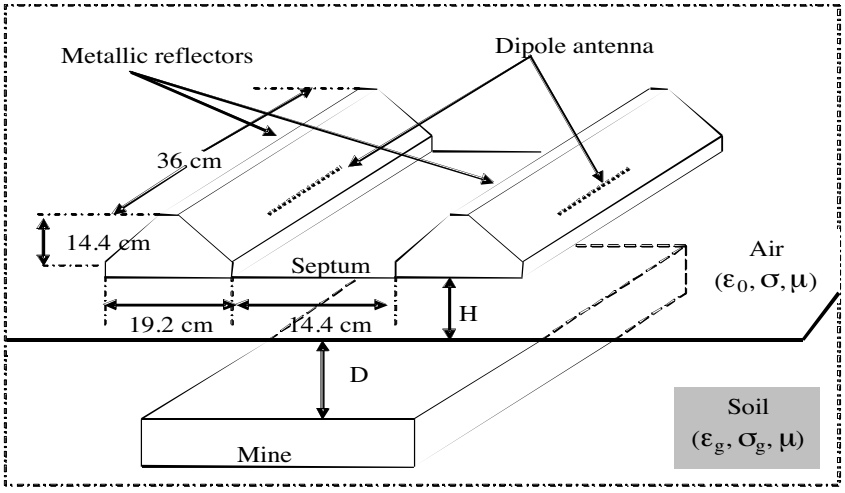

Figure 1. Construction and dimensions of a separated-aperture sensor designed for detecting land mines.

3. MODELING THE SEPARATED-APERTURE SENSOR GPR SYSTEM USING FDTD

One of the most efficient and commonly used methods for the analysis of microwave detection of buried objects is the FDTD method [14]. The FDTD algorithm is used to simulate and analyze the separated-aperture sensor. The overall model used in this paper is shown in Fig. 2, the finite computational volume, which contains the sensor, lossy ground, and mine, is truncated with an 8-cell absorbing boundary condition (ABC): Brenger's split-field perfectly matched layer [7–10]. The FDTD lattice dimensions are $60 \times 90 \times 140$ cm, which is comprised of cubic Yee cells each of dimension 1.2 cm. This discritization is appropriate for electromagnetic simulation in the frequency band 600–1000 MHz. Field components are updated every 23.094011 ps; this time step satisfies the condition for numerical stability stated by Courant [7]. Each reflector has a 19.2 cm (16-cell) width in the y-direction, 36 cm (30-cell) depth in x-direction, and 14.4 cm (12-cell) heights in z-direction. A conducting staircase model of $\sigma = 10^{16}$ S/m is used to represent the reflectors. The reflectors are separated by a septum of 14.4 cm width (12-cell) which is modeled as a conductor plate of $\sigma = 10^{16}$ S/m. Dipole antennas of 15.6 cm (13 cells) length are used. A thin wire is used to model the dipole antenna [11]. The feeding gap of a thin-wire antenna is often modeled in FDTD method, by the

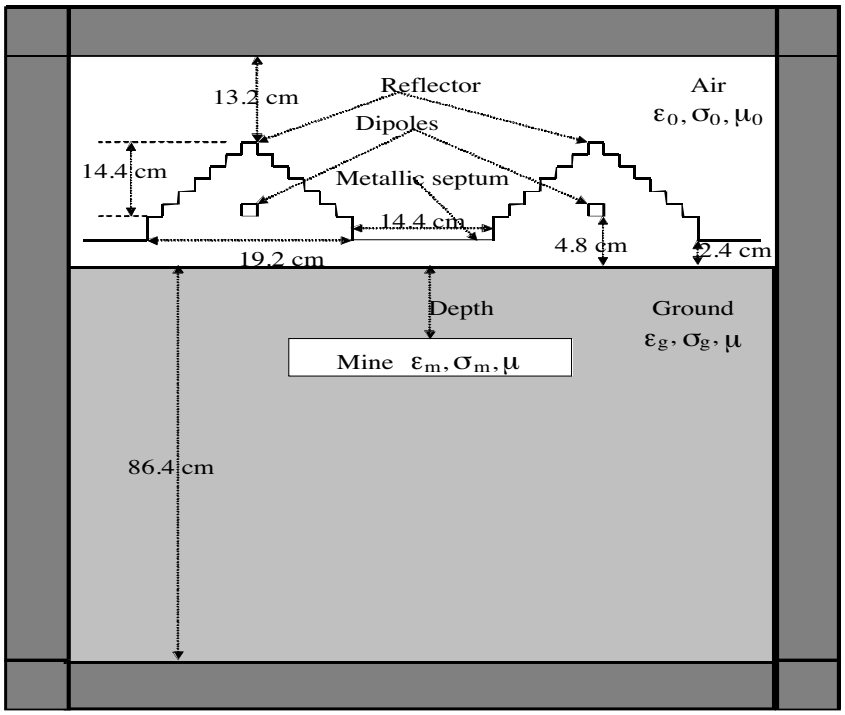

Figure 2. FDTD model for separated-aperture sensor GPR system over a ground with a buried target.

so-called "on-cell gap" which lets the feeding gap be one cell of Yee's lattice. However, the actual feeding gap is usually smaller than the cell size. The conventional one-cell gap model can therefore cause cell-size dependent error in FDTD computation [12]. This problem is treated in [12] by assuming an infinitesimal feeding gap instead of a one-cell gap. In this method, a new gap model for FDTD calculation is considered in which the antenna gap is infinitesimally small.

4. RESULTS AND DISCUSSION

The results are obtained when a ramped sinusoidal source is applied at the dipole center of the transmitting antenna of a separated-aperture sensor placed at a height of 2.4 cm over empty ground and at the same height over the same ground containing a buried target. The FDTD algorithm runs for a period of time long enough for the fields every-where to reach the steady state. Two types of ground soils

are considered; the first one is described as a "fairly dry, loamy soil with moisture content by weight of 6%" and has the following electrical properties: $\varepsilon_r = 2.9$, $\mu_r = 1.0$, $\sigma = 0.02\,\mathrm{S/m}$ [6], while the second is "red clay soil with 9.6% water by dry weight" and has $\varepsilon_r = 8.1$, $\mu_r = 1.0$, $\sigma = 0.038\,\mathrm{S/m}$ [6]. All targets selected for the following presentations and discussion are box-shaped and have the dimensions $30 \times 30 \times 7.2\,\mathrm{cm}$.

4.1. Metallic Mine Detection

The metallic mine is represented by a conductor block with the following electrical properties: $\varepsilon_r = 1.0$, $\mu_r = 1.0$, $\sigma = 10^{16}\,\mathrm{S/m}$.

Fig. 3 shows the coupling between the transmitting and receiving antenna $|S_{21}|$ for the sensor when it is placed over empty fairly dry soil and when it is placed over the same type of soil inside which a metallic mine is buried at depth of 12 cm. As shown in this figure, there is a considerable increase in $|S_{21}|$ over the frequency band 600–1000 MHz due to the presence of the bureid target. The optimum frequency at which a metallic mine can be detected when buried in such a soil is 800 MHz. At this frequency there is about 28 dB increase in $|S_{21}|$ due to the existence of the metallic target.

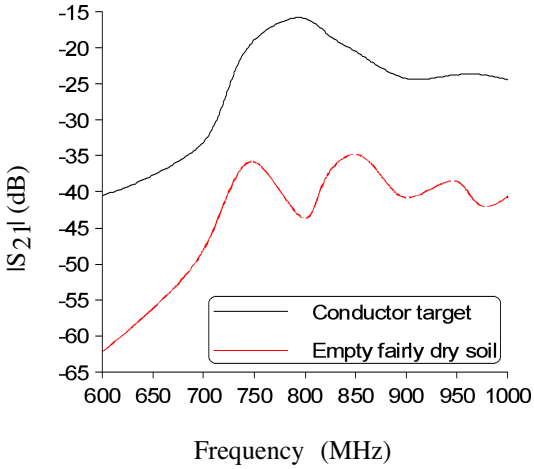

Figure 3. Coupling between the sensor antennas when it is placed over empty fairly dry soil (no target) and over the same soil with a conductor block of dimensions $30 \times 30 \times 7.2\,\mathrm{cm}$ buried at 12 cm depth.

Fig. 4 shows the coupling between the transmitting and receiving antenna $|S_{21}|$ for the sensor when it is placed over empty red clay soil

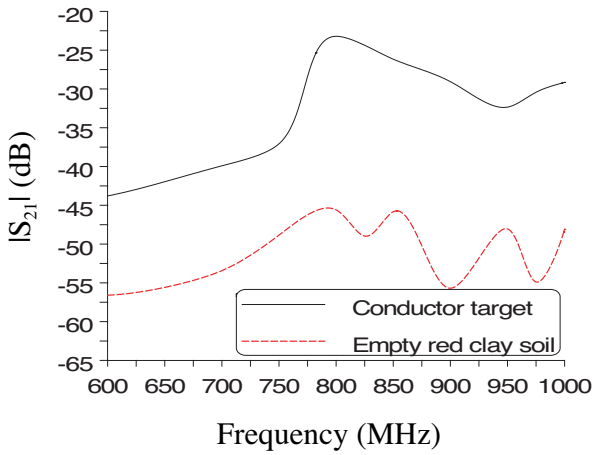

Figure 4. Coupling between the sensor antennas when it is placed over empty red clay soil (no target) and over the same soil with a conductor block of dimensions $30 \times 30 \times 7.2$ cm buried at 12 cm depth.

and when it is placed over the same type of soil inside which a metallic mine is buried at depth of 12 cm. As shown in this figure, there is a considerable increase in $|S_{21}|$ over the frequency band 600–1000 MHz due to the existence of the target. The optimum frequency at which a metallic mine can be detected when buried in such a soil is 800 MHz. At this frequency there is about 23 dB increase in $|S_{21}|$ due to the existence of the metallic mine.

Figures 5 and 6 show the frequency-domain electric field distribution of E_x component in the ground and inside the reflectors of the sensor in the case of an empty soil and that of the same soil with a buried metallic mine at depth of 12 cm, respectively. By comparing the figures, it becomes clear that the existence of a metallic mine results in a significant increase in the electric field at the receiving antenna.

4.2. Dielectric Mine Detection

Two types of dielectric targets are considered; the first one is described as "plexiglass block" and has the following electrical properties: $\varepsilon_r = 2.6$, $\mu_r = 1.0$, $\sigma \approx 0.0$, while the second is "stycast block" and has $\varepsilon_r = 7.4$, $\mu_r = 1.0$, $\sigma \approx 0.0$ [6].

Fig. 7 shows the coupling between the transmitting and receiving antennas $|S_{21}|$ for the sensor when it is placed over empty fairly dry soil and when it is placed over the same type of soil inside which a plexiglass block is buried at depth of 16.8 cm. As shown in this figure,

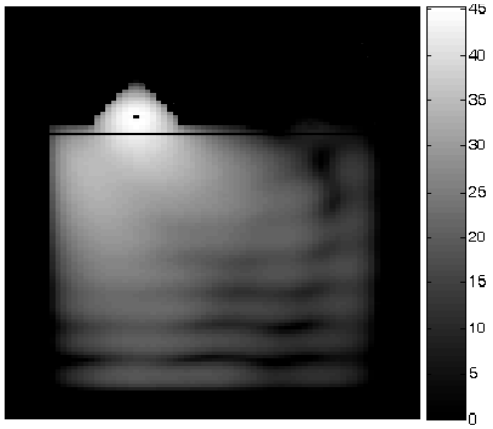

Figure 5. Electric field intensity distribution in the frequency-domain inside an empty fairly dry soil and in the reflectors of the sensor, $f = 800\,\text{MHz}$.

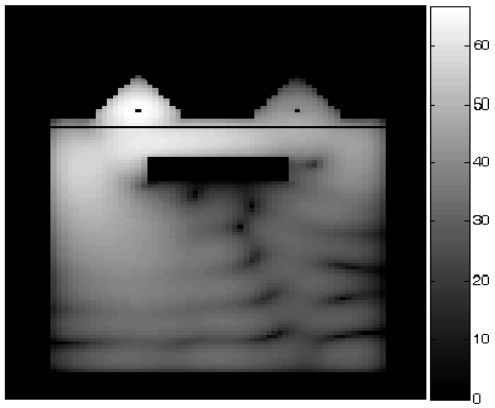

Figure 6. Electric field intensity distribution in the frequency-domain inside a fairly dry soil containing a metallic target buried at a depth of 12 cm and in the reflectors of the sensor, $f = 800\,\text{MHz}$.

there is an insignificant increase in $|S_{21}|$ in some frequency bands. The optimum frequency band at which a plexiglass block can be detected when buried in such a soil is 750–850 MHz with maximum detectability at 800 MHz. At this frequency there is about 10 dB increase in $|S_{21}|$ due to the existence of the plexiglass block as shown in Fig. 8.

Fig. 9 shows the coupling between the transmitting and receiving antennas $|S_{21}|$ for the sensor when it is placed over empty red clay

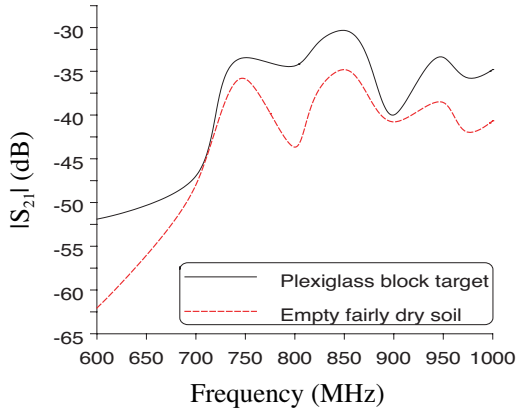

Figure 7. Coupling between the sensor antennas when it is placed over empty fairly dry soil (no target) and over the same soil with a plexiglass block of dimensions $30 \times 30 \times 7.2$ cm buried at 16.8 cm depth.

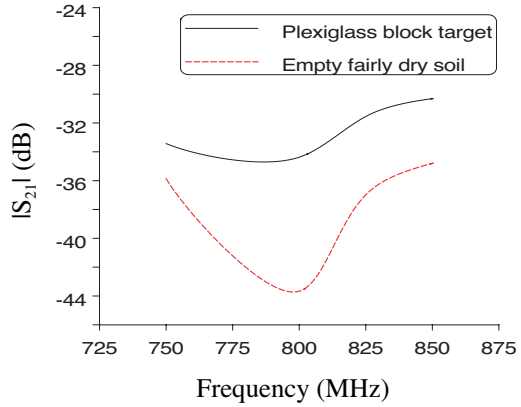

Figure 8. Coupling between the sensor antennas when it is placed over empty fairly dry soil (no target) and over the same soil with a plexiglass block of dimensions $30 \times 30 \times 7.2$ cm buried at 16.8 cm depth, $f = 750$–850 MHz.

soil and when it is placed over the same type of soil inside which a plexiglass block is buried at depth of 16.8 cm. As shown in this figure, there is a considerable increase in $|S_{21}|$ over the frequency band 600–1000 MHz. The optimum frequency at which a plexiglass block can be detected when buried in such a soil is 827 MHz. At this frequency there is about 28 dB increase in $|S_{21}|$ due to the existence of the plexiglass

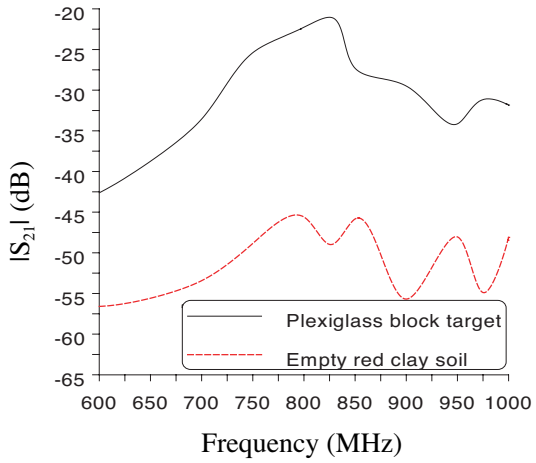

Figure 9. Coupling between the sensor antennas when it is placed over empty red clay soil (no target) and over the same soil with a plexiglass block dimensions $30 \times 30 \times 7.2$ cm buried at 16.8 cm depth.

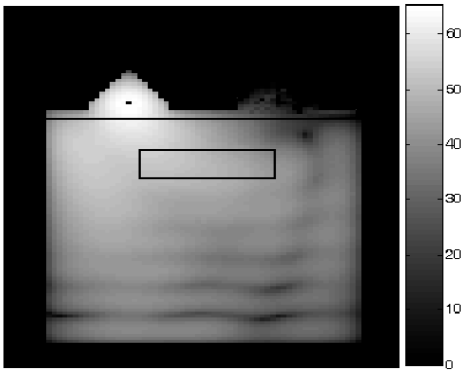

Figure 10. Electric field intensity distribution in the frequency-domain inside a fairly dry soil containing a plexiglass block buried at a depth of 16.8 cm and in the reflectors of the sensor, $f = 800$ MHz.

block.

Figures 10 and 11 show the frequency-domain electric field distribution E_x component in the ground and inside the reflectors of the sensor in the cases of plexiglass block buried in fairly dry soil and red clay soil, respectively.

Comparing Fig. 10 with 5, it becomes clear that the existence of a plexiglass block results in a little increase of the electric field at

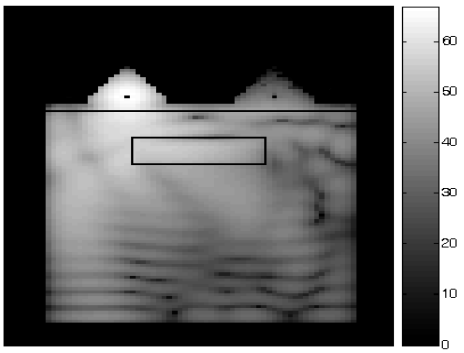

Figure 11. Electric field intensity distribution in the frequency-domain inside a red clay soil containing a plexiglass block buried at a depth of 16.8 cm and in the reflectors of the sensor, $f = 800$ MHz.

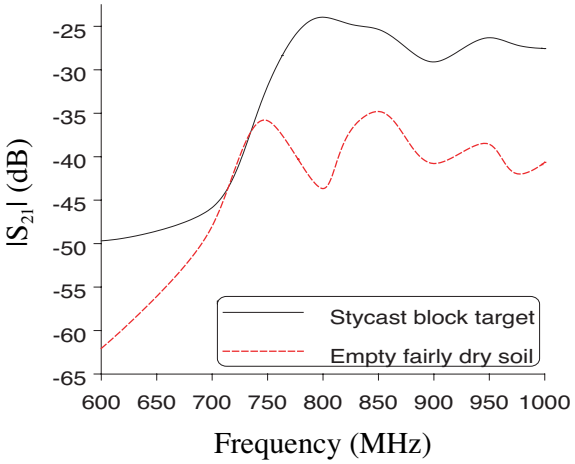

Figure 12. Coupling between the sensor antennas when it is placed over empty fairly dry soil (no target) and over the same soil with a stycast block of dimensions $30 \times 30 \times 7.2$ cm buried at 12 cm depth.

the receiving antenna because the relative permittivity of the plexiglass block is near to that of a fairly dry soil inside which it is buried ($\varepsilon_r = 2.6$ versus $\varepsilon_r = 2.9$, respectively).

Fig. 12 shows the coupling between the transmitting and receiving antennas $|S_{21}|$ for when the sensor is placed over empty fairly dry soil and when it is placed over the same type of soil with a stycast block buried at depth of 12 cm. The optimum frequency band at which

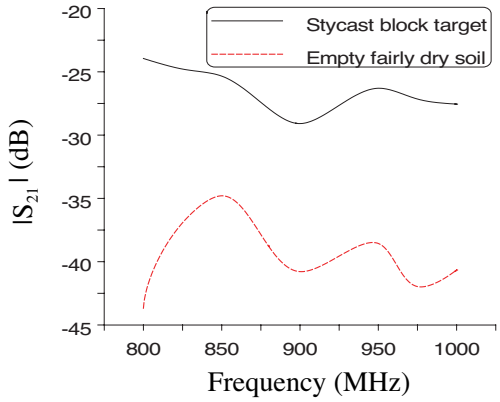

Figure 13. Coupling between the sensor antennas when it is placed over empty fairly dry soil (no target) and over the same soil with a stycast block of dimensions $30 \times 30 \times 7.2$ cm buried at 12 cm depth, $f = 800$–1000 MHz.

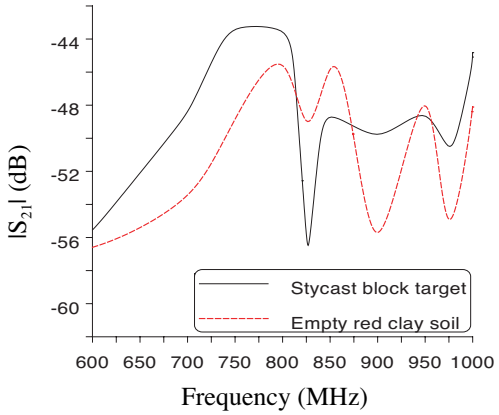

Figure 14. Coupling between the sensor antennas when it is placed over empty red clay soil (no target) and over the same soil with a stycast block of dimensions $30 \times 30 \times 7.2$ cm buried at 12 cm depth.

a stycast block can be detected when buried in such a soil is 800–1000 MHz with maximum detectability at 800 MHz. At this frequency there is about 20 dB increase in $|S_{21}|$ due to the existence of the stycast block as shown in Fig. 13.

Fig. 14 shows the coupling between the transmitting and receiving antennas $|S_{21}|$ when the sensor is placed over empty red clay soil and when it is placed over the same type of soil with a stycast block buried

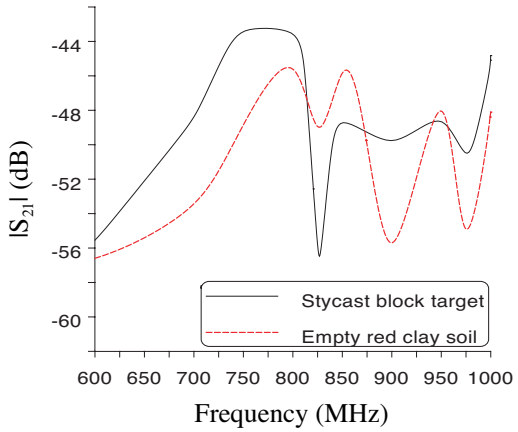

Figure 15. Coupling between the sensor antennas when it is placed over empty red clay soil (no target) and over the same soil with a stycast block of dimensions $30 \times 30 \times 7.2$ cm buried at 12 cm depth, $f = 700$–800 MHz.

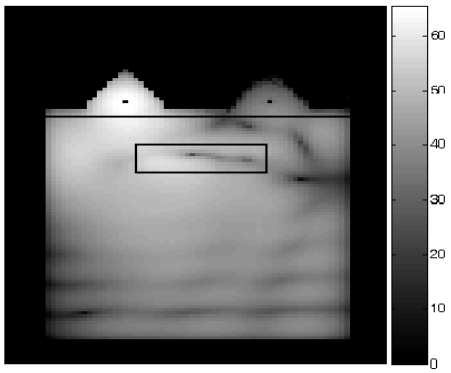

Figure 16. Electric field intensity distribution in the frequency-domain inside a fairly dry soil containing a stycast block buried at a depth of 12 cm and in the reflectors of the sensor, $f = 800$ MHz.

at depth of 12 cm. The optimum frequency band at which a stycast block can be detected when buried in such a soil is 700–800 MHz with maximum detectability at 750 MHz. At this frequency there is about 6 dB increase in $|S_{21}|$ due to the existence of the stycast block as shown in Fig. 15.

Figures 16 and 17 show the frequency-domain electric field distribution of E_x component in the ground and inside the reflectors

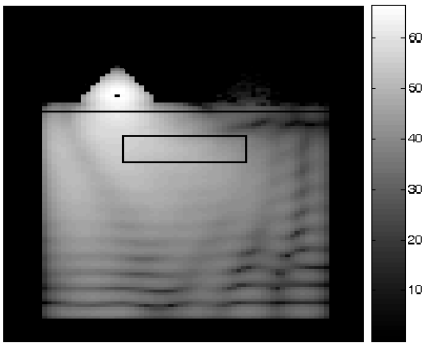

Figure 17. Electric field intensity distribution in the frequency-domain inside a red clay soil containing a stycast block buried at a depth of 12 cm and in the reflectors of the sensor, $f = 800$ MHz.

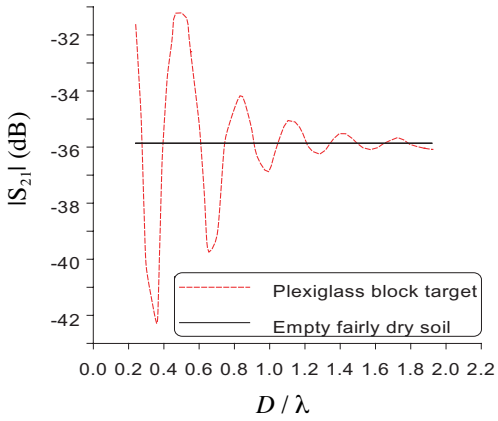

Figure 18. Coupling between the sensor antennas when a plexiglass block target is buried in a fairly dry soil versus its depth per wavelength, $f = 750$ MHz.

of the sensor in the cases of stycast block buried in fairly dry soil and red clay soil, respectively.

A comparison between Figures 16 and 5 shows that the existence of a stycast block results in a significant increase in the electric field at the receiving antenna because the relative permittivity of the stycast block is much different from that of the fairly dry soil inside which it is buried ($\varepsilon_r = 7.4$ versus $\varepsilon_r = 2.9$, respectively).

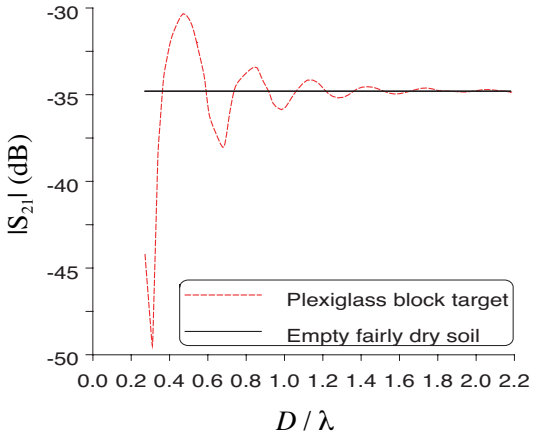

Figure 19. Coupling between the sensor antennas when a plexiglass block target is buried in fairly dry soil versus its depth, $f = 850\,\text{MHz}$.

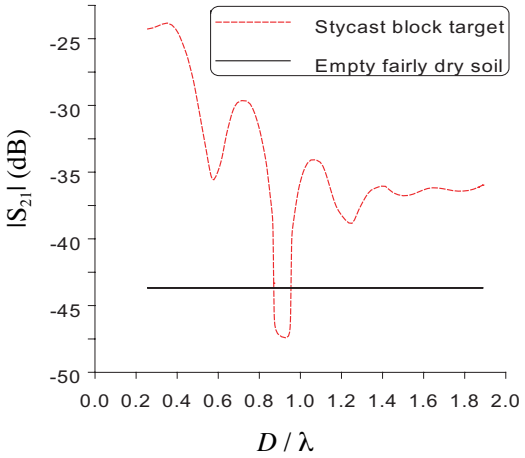

Figure 20. Coupling between the antennas when a stycat block target is buried in a fairly dry soil versus its depth, $f = 800\,\text{MHz}$.

4.3. Dependence of Target Detectability on Depth of Buried Target below Ground Surface

Figures 18 and 19 show the dependence of $|S_{21}|$ when a plexiglass block is buried in a fairly dry soil on the target depth given as a ratio to the wavelength at: 750 MHz and 850 MHZ, respectively. As shown in these figures, the coupling between the two antennas is affected by the target

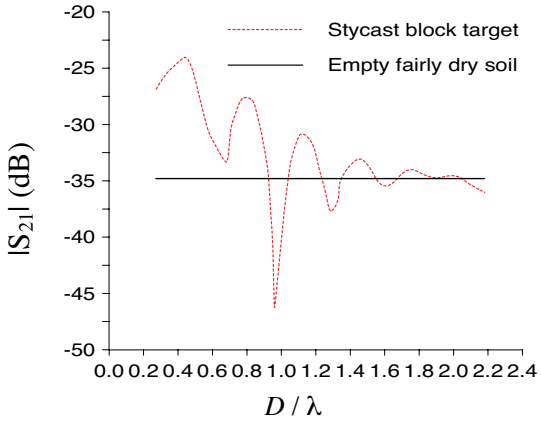

Figure 21. Coupling between the sensor antennas when a stycat block target is buried in a fairly dry soil versus its depth, $f = 850\,\text{MHz}$.

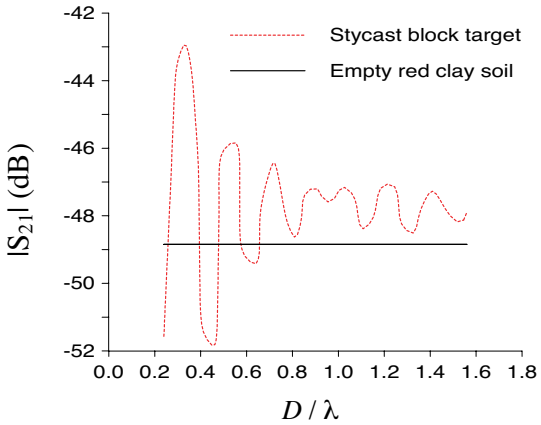

Figure 22. Coupling is being between the sensor antennas when a stycat block target is buried in red clay soil versus its depth, $f = 800\,\text{MHz}$.

depth so that, as the target depth increases the coupling coefficient converges to that in case of empty ground. There are some depths at which the target can not be detected depending on the operating frequency of the sensor.

Figures 20 and 21 show the dependence of $|S_{21}|$ when a stycast block target is buried in a fairly dry soil on the target depth given as a ratio to the wavelength at: 800 MHz and 850 MHz,

respectively. As shown in these figures; there is a distinct change in the coupling between the two antennas with changing the depth of the target however, as the target depth increases the coupling coefficient converges to that in case of empty ground. There are some depths at which the target can not be detected these depths depending on the operating frequency of the sensor.

Figure 22 shows the dependence of $|S_{21}|$ when a stycast block target is being buried in a red clay soil on the target depth given as a ratio to wavelength at 750 MHz. As shown in these figures; there is a distinct change in the coupling between the two antennas with changing the depth of the target however, as the target depth increases the coupling coefficient converges to that in case of empty. There are some depths at which the target can not be detected depending on the operating frequency of the sensor.

5. CONCLUSION

The capability of the separated-aperture sensor to detect buried targets is examined by evaluating and comparing the electromagnetic coupling between its transmitting and receiving antennas in the presence and absence of a buried target while the system is being placed over the ground. The results concerning the coupling between the transmitting and receiving antennas are presented considering various practical parameters such as the operating frequency, the electric properties of the ground soil and the buried target, and the depth at which the target is buried under the ground surface. It is shown that target detectability using the separated-aperture sensor is strongly dependent on all of the above parameters.

REFERENCES

1. Bourgeois, J. M. and G. S. Smith, "A fully three-dimensional simulation of a ground-penetrating-radar: FDTD theory compared with experiment," *IEEE Trans. Geos. Remote Sensing*, Vol. 34, 36–44, January 1996.
2. Nishioka, Y., O. Maeshima, T. Uno, and S. Adachi, "FDTD analysis of resistor-loaded bow-tie antennas covered with ferrite-coated conducting cavity for subsurface radar," *IEEE Tarns. Antennas Propagat.*, Vol. 47, 970–997, June 1999.
3. Montoya, T. P. and G. S. Smith, "Land mine detection using a ground-penetrating radar based on resistively loaded Vee dipoles," *IEEE Trans. Antennas Propagat.*, Vol. 47, 1795–1806, December 1999.

4. Montoya, T. P. and G. S. Smith, "A study of pulse radiation from several broad-band loaded monopoles," *IEEE Trans. Antennas Propagat.*, Vol. 44, 1172–1182, August 1996.
5. Lee, K.-H., C.-C. Chen, F. L. Texeira, and R. Lee, "Modeling and investigation of a geometrically complex UWB GPR antenna using FDTD," *IEEE Trans. Antennas Propagat.*, Vol. 52, 1983–1991, August 2004.
6. Bourgeois, J. M. and G. S. Smith, "A complete electromagnetic simulation of the separated-aperture sensor for detecting buried land mines," *IEEE Trans. Antennas Propagat.*, Vol. 46, 1419–1426, October 1998.
7. Taflove, A. and S. Hagness, *Computational Electrodynamics: The Finite-Difference Time-Domain Method*, 2nd edition, Artech House, 2000.
8. Brenger, J. P., "A perfectly matched layer for the absorption of electromagnetic waves," *J. Computational Physics*, Vol. 114, 185–200, 1994.
9. Brenger, J. P., "Three-dimensional perfectly matched layer for the absorption of electromagnetic waves," *J. Computational Physics*, Vol. 127, 363–379, 1996.
10. Brenger, J. P., "Perfectly matched layer for the FDTD solution of wave-structure interaction problems," *IEEE Trans. Antennas and Propagation*, Vol. 51, 110–117, 1996.
11. Kunz, K. and R. J. Luebbers, *The Finite-Difference Time-Domain Method for Electromagnetics*, CRC Press, 1993.
12. Watanabe, S.-I. and M. Taki, "An improved FDTD model for the feeding gap of a thin-wire antenna," *IEEE Microwave And Guided Wave Letters*, Vol. 8, No. 4, 152–154, April 1998.
13. Qu, S. and C. Ruan, "Effect of round corners on bowtie antennas," *Progress In Electromagnetics Research*, PIER 57, 179–195, 2006.
14. Chen, X., K. Huang, and X.-B. Xu, "Microwave imaging of buried inhomogeneous objects using parallel genetic algorithm combined with FDTD method," *Progress In Electromagnetics Research*, PIER 53, 283–298, 2005.
15. Uduwawala, D., M. Norgren, P. Fuks, and A. Gunawardena, "A complete FDTD simulation of a real GPR antenna system operating above lossy and dispersive grounds," *Progress In Electromagnetics Research*, PIER 50, 209–229, 2005.